Dynamic coupling of subsurface and seepage flows solved within a regularized partition formulation

Jean Marçais, Jean-Raynald de Dreuzy, Jocelyne Erhel

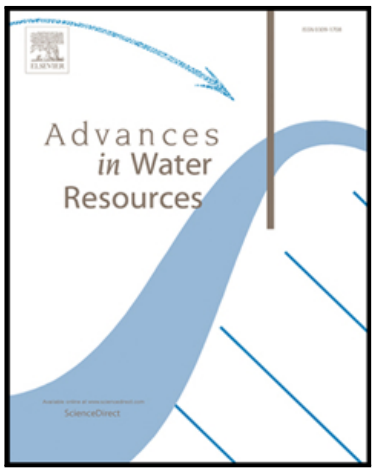

Dynamic coupling of subsurface and seepage flows solved within a regularized partition formulation

J. Marçais, J.-R. de Dreuzy, J. Erhel

PII: S0309-1708(17)30310-X
DOI: 10.1016/j.advwatres.2017.09.008
Reference: ADWR 2941

To appear in: *Advances in Water Resources*

Received date: 12 April 2017
Revised date: 6 September 2017
Accepted date: 6 September 2017

Please cite this article as: J. Marçais, J.-R. de Dreuzy, J. Erhel, Dynamic coupling of subsurface and seepage flows solved within a regularized partition formulation, *Advances in Water Resources* (2017), doi: 10.1016/j.advwatres.2017.09.008

Highlights

- Integrating seepage dynamic in subsurface flow modeling at the hillslope scale.
- Coupling storage variation and seepage through a robust partition formulation.
- Smooth convex regularization of seepage onset, sharp seepage retreat.
- Numerical application and demonstration of hillslope storage Boussinesq equations.

Dynamic coupling of subsurface and seepage flows solved within a regularized partition formulation

J. Marçais[1a,b], J.-R. de Dreuzy[b,], J. Erhel[c,]

[a]*Agroparistech, 16 rue Claude Bernard, 75005 Paris, France*
[b]*Géosciences Rennes (UMR 6118 CNRS), Université de Rennes 1, Campus de Beaulieu, 35042 Rennes Cedex, France*
[c]*INRIA Rennes-Bretagne Atlantique, campus de Beaulieu, 35042 Rennes, France*

Abstract

Hillslope response to precipitations is characterized by sharp transitions from purely subsurface flow dynamics to simultaneous surface and subsurface flows. Locally, the transition between these two regimes is triggered by soil saturation. Here we develop an integrative approach to simultaneously solve the subsurface flow, locate the potential fully saturated areas and deduce the generated saturation excess overland flow. This approach combines the different dynamics and transitions in a single partition formulation using discontinuous functions. We propose to regularize the system of partial differential equations and to use classic spatial and temporal discretization schemes. We illustrate our methodology on the 1D hillslope storage Boussinesq equations (Troch et al., 2003). We first validate the numerical scheme on previous numerical experiments without saturation excess overland flow. Then we apply our model to a test case with dynamic transitions from purely subsurface flow dynamics to simultaneous surface and subsurface flows. Our results show that discretization respects mass balance both locally and globally, converges when the mesh or time step are refined. Moreover the regularization parameter can be taken small enough to ensure accuracy without suffering of numerical artifacts. Applied to some hundreds of realistic hillslope cases taken from Western side of France (Brittany), the developed method appears to be robust and efficient.

[1]Corresponding author: jean.marcais@polytechnique.edu

Keywords: Subsurface flow, Saturation Excess, Seepage, ODE with discontinuous right-hand side, Regularization, Boussinesq equations

1. Introduction

Under the same term, runoff gathers several processes of different origins including infiltration excess overland flow and saturation excess overland flow (Kirkby, 1978; Bonell, 1998; Horton, 1933; McGlynn et al., 2002; Freeze & Harlan, 1969). While infiltration excess overland flow is controlled by rainfall intensity and surface properties like roughness (Horton, 1933; Smith & Goodrich, 2006; Darboux et al., 2002), saturation excess overland flow is generated by subsurface flow and saturation dynamics (Dunne & Black, 1970; Sophocleous, 2002). It occurs locally in so-called saturated source areas (Ogden & Watts, 2000) when the soil column is saturated up to the surface (Dunne, 1978; Musy & Higy, 2004). It comes from precipitation that cannot infiltrate (sometimes called direct precipitations onto saturated areas) and from subsurface flows that exfiltrate and return to the surface, i.e. seepage flow or return flow (Dunne & Black, 1970). Once the soil column remains fully saturated, the subsurface flux stabilizes, remaining equal to the product of the soil transmissivity by the local hydraulic gradient. At the surface, fluxes can be highly variable depending on exfiltration and precipitations dynamics. Saturated source areas are found at the bottom of slopes, in the vicinity of rivers, in wetlands where water table can quickly rise up to the surface as well as upslope in slope hollows that force

flowpaths to converge and exfiltrate (Fan & Bras, 1998; Troch et al., 2002; Brutsaert, 2005; Birkel et al., 2015). Subsurface and saturation excess overland flow have been proven to be important for providing water for evapotranspiration (Maxwell & Condon, 2016), enhancing erosion (Fox & Wilson, 2010), increasing groundwater flooding risks (Holman et al., 2009; Kreibich & Thieken, 2008; Habets et al., 2010; Bauer et al., 2006; Miguez-Macho & Fan, 2012), shaping the residence time distribution (Tetzlaff et al., 2014; Rinaldo et al., 2015; Harman, 2015) maintaining anoxic conditions in the soil and promoting denitrification hotspots (Pinay et al., 2015).

There is a sharp transition when infiltration and subsurface flows do no longer sustain the full saturation of the soil column (Vivoni et al., 2007). Overland flow vanishes, a partially saturated area develops in lieu of the saturated source area, the water table falls down below the surface and subsurface flow becomes dynamic and non-linearly dependent on saturation. Such transitions between so-called fully saturated and partially saturated regimes are spatially variable and dynamic. They have been modeled by coupling shallow water and groundwater equations (LaBolle et al., 2003; Barthel & Banzhaf, 2016; Camporese et al., 2010) either by an exchange of fluxes (Govindaraju & Kavvas, 1991; Panday & Huyakorn, 2004; Markstrom et al., 2008) or by assigning the shallow water equations as a boundary to the groundwater equations (Kollet & Maxwell, 2006). Another method is to solve the groundwater equations for a prescribed position

of the saturated source areas (Bresciani et al., 2014, 2016; Beaugendre et al., 2006) and to iterate until convergence is met (Diersch, 2013; Harbaugh, 2005). The seepage front (defined as the intersection of the subsurface water table with the land surface) is deduced accordingly (Anderson et al., 2015; Batelaan & De Smedt, 2004) and saturation excess overland flow is eventually derived from mass balance computations.

While these integrated hydrological surface-subsurface models (for a comprehensive review, see Fatichi et al. (2016)) are adapted to well instrumented catchments or critical zone observatories, they require high computation capacities (Putti & Paniconi, 2004) and a lot of data to be calibrated with (Reggiani et al., 1998) making them difficult to parametrize because of their long run time. They are also prone to equifinality issues (Beven, 2006) and are sometimes subject to numerical instabilities (Doherty & Christensen, 2011). For applications where the only available information are a DEM, the rainfall time series and a discharge time series, non intensive process-based models have been proposed (Troch et al., 2003; Broda et al., 2012) but, to the best of our knowledge, they do not take into account the non linearity, described above, coming from the dynamic interactions between the water table and the land surface.

Here, we propose an integrated approach to simultaneously solve the subsurface flow, locate the potential saturated source areas and deduce the generated saturation excess overland flow. This approach is well suited to the sharp

transitions presented previously. We hypothesize that surface processes can be simplified as follows. We assume instantaneous flood routing as surface flows are some orders of magnitude faster than subsurface flows (Dunne & Black, 1970; Fan & Bras, 1998). We consider reinfiltration processes as negligible. In temperate climates, most of the saturation excess overland flow occurs downhill and only a small amount of this flow is likely to reinfiltrate (Musy & Higy, 2004).

We model subsurface flow with the Boussinesq hydraulic groundwater theory based on Darcy's law and Dupuit-Forchheimer assumption (Boussinesq, 1877; Brutsaert, 2005; Troch et al., 2013). It expresses that hydraulic head responds to flow through transmissivity feedbacks without inertial effects (Rodhe, 1987; Bishop et al., 2011). We work at the hillslope scale with the hillslope storage Boussinesq equations (Troch et al., 2003), which include the geologic, pedologic and geomorphologic controls on subsurface flow dynamics (Bachmair & Weiler, 2012; Savenije, 2010; Freer et al., 1997; Lanni et al., 2013). They indeed model subsurface flow at the soil/bedrock interface (Freer et al., 2002; Tromp-van Meerveld & McDonnell, 2006), which is the most likely to generate saturation excess overland flow in humid and steep terrains with conductive soils (Weiler et al., 2006). They have also been extended to model the coupling between shallow and deep groundwater flow (Broda et al., 2012).

First, we describe the partially saturated and fully saturated flow regimes

that can be encountered on hillslopes following the two cases of Fan & Bras (1998) (section 2.1) and combine them in a partial differential system deriving from partition considerations (section 2.2). We regularize this system for numerical integration, discretize it spatially with a mixed finite element scheme and obtain a system of differential equations (section 2.3). Second, we validate the method and analyze its convergence properties (sections 3.1 and 3.2). Finally we discuss its efficiency and robustness on realistic hillslope cases (section 3.3).

2. Methods

We first recall the hillslope storage Boussinesq equations (Troch et al., 2003; Hilberts et al., 2004; Paniconi et al., 2003) and add to them the overflow condition when saturation reaches the surface. We show how the two regimes of partial and total saturation are generally formalized and further propose an alternative integrated partition formulation. The issued differential discontinuous equations are then regularized for numerical integration and spatially discretized with a mixed finite element scheme.

2.1. Hillslope storage Boussinesq equations

2.1.1. Case 1: Subsurface flow only

Below land surface, when the soil is not fully saturated, only subsurface flow occurs. Hillslope storage Boussinesq equations physically describe the relation

between subsurface flow and saturation (Troch et al. (2003), case 1 of Figure 1a). Following Dupuit-Forchheimer assumption, discharge is proportional to the saturated thickness. Discharge is further integrated transversally to the main slope direction to yield a 1D continuity problem where discharge is also proportional to the width w [m] of the transect profile (Figure 1b). The other key physical characteristic of the hilllslope is its slope θ [rad] describing the mean evolution of the soil layer height. The integrated flux over the transect $Q(x,t)$ [m^3 s^{-1}] is linked to the subsurface water storage $S(x,t)$ [m^2] through the following set of equations:

$$\begin{cases} \dfrac{\partial S}{\partial t}(x,t) &= -\dfrac{\partial Q}{\partial x}(x,t) + N(t)\,w(x) \\ Q(x,t) &= -\dfrac{kS(x,t)}{f}\left(\cos\theta\ \dfrac{\partial}{\partial x}\left(\dfrac{S}{fw}\right)(x,t) + \sin\theta\right) \\ 0 &\leq S(x,t) \leq S_c(x) \\ S(x,t) < S_c(x) \ \ \textbf{or} \ \ & -\dfrac{\partial Q}{\partial x}(x,t) + N(t)\,w(x) < 0 \ , \end{cases} \tag{1}$$

where x [m] represents the distance to the channel varying between 0 at the river and L at the water divide, N [m s^{-1}] is the infiltration, k [m s^{-1}] is the hydraulic conductivity, f [-] is the drainable porosity. The subsurface water storage $S(x,t)$ is defined in Troch et al. (2003) by $S(x,t) = f\,w(x)\,h(x,t)$ where h is the groundwater elevation height [m] (Figure 1). $S(x,t)$ cannot exceed the maximum subsurface water storage S_c [m^2] defined by $S_c(x) = f\,w(x)\,d$

where d [m] is the soil depth. For illustration purposes and with no loss of generality, we assume in what follows that k, f, θ and d are constant. The first equation of system (1) is the mass balance equation stating that the temporal variation of storage results from the local variation of subsurface flows and from the infiltration. The second line is Darcy's equation, integrated vertically and laterally, written as a function of the subsurface water storage S. The third equation just reminds that S is positive and cannot exceed the maximum subsurface water storage S_c. This system applies as long as the condition of the fourth line is fulfilled, i.e. for partially saturated soil columns ($S(x,t) < S_c(x)$) or for fully saturated soil columns desaturating ($-\dfrac{\partial Q}{\partial x}(x,t) + N(t)\, w(x) < 0$).

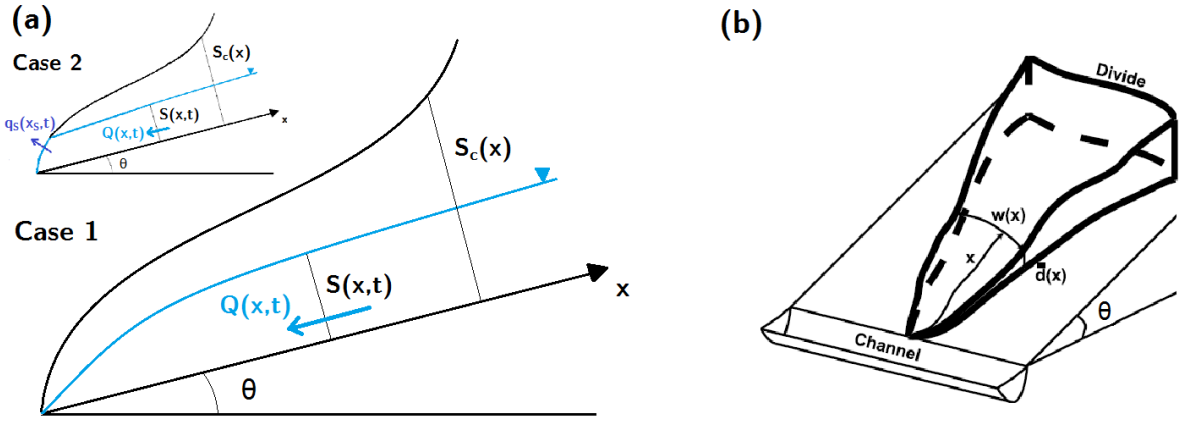

Figure 1: (a) Cross-section view of the hillslope with a constant slope θ. The water table location $S(x,t)$ is indicated in blue. The subsurface flux $Q(x,t)$ is marked by the blue arrow. The saturation excess overland flow $q_S(x_S,t)$ (case 2) is materialized by the purple arrow and the surface by $S_c(x)$. Cases 1 and 2 represent partially saturated and locally fully saturated hillslopes respectively. (b) 3D view of the hillslope with an illustration of the width function $w(x)$ (Adapted from Troch et al. (2003)).

157 *2.1.2. Case 2: Subsurface flow and dynamic saturation excess overland flow*

158 If, at the location x_S, the soil is fully saturated and there is a positive flux
159 balance, the excess in the flux balance is identified to the saturation excess
160 overland flow q_S [m^2 s^{-1}] as it cannot be assigned to storage temporal variations
161 ($\frac{\partial S}{\partial t}(x_S, t) = 0$, case 2 of Figure 1a). The system of equations becomes:

$$\begin{cases} q_S(x_S,t) &= -\dfrac{\partial Q}{\partial x}(x_S,t) + N(t)\, w(x_S) \\ \dfrac{\partial S}{\partial t}(x_S,t) &= 0 \\ Q(x_S,t) &= -\dfrac{kS_c(x_S)}{f}\left(\cos\theta\, \dfrac{\partial}{\partial x}\left(\dfrac{S_c}{fw}\right)(x_S,t) + \sin\theta\right) \\ S(x_S,t) &= S_c(x_S) \textbf{ and } -\dfrac{\partial Q}{\partial x}(x_S,t) + N(t)\, w(x_S) \geq 0 \ . \end{cases} \tag{2}$$

162 The fourth line ensures that the soil is fully saturated and that there is a positive
163 flux balance ($-\frac{\partial Q}{\partial x}(x_S, t) + N(t)\, w(x_S) \geq 0$). As shown by the first equation,
164 saturation excess overland flow is made up of two terms representing the seepage
165 flow ($-\frac{\partial Q}{\partial x}$) and the direct precipitations onto saturated areas ($N\, w$) (Dunne
166 & Black, 1970).

167 Solving the dynamic transition between these two regimes (essentially due
168 to interactions between the soil water table and the land surface) requires to
169 change of system of equations (system (1) or (2)) depending on the state of
170 saturation and subsurface flow (S and Q). It is the last equation in systems (1)

and (2) that controls the transition.

2.2. Partition Problem

To avoid switching between regimes and equation sets, we propose an alternative partition formulation. This formulation reconciles systems (1) and (2) in a single system by partitioning the incoming flux $-\frac{\partial Q}{\partial x} + N\,w$ in the variation of the subsurface water storage $\frac{\partial S}{\partial t}$ and in the saturation excess overland flow q_S :

$$\begin{cases} \dfrac{\partial S}{\partial t}(x,t) + q_S(x,t) &= -\dfrac{\partial Q}{\partial x}(x,t) + N(t)\,w(x) \\ \\ q_S(x,t) &= \mathscr{G}\left(\frac{S(x,t)}{S_c(x)}\right)\mathscr{R}\left(-\dfrac{\partial Q}{\partial x}(x,t) + N(t)\,w(x)\right) \\ \\ Q(x,t) &= -\dfrac{kS(x,t)}{f}\left(\cos\theta\ \dfrac{\partial}{\partial x}\left(\dfrac{S}{fw}\right)(x,t) + \sin\theta\right) \\ \\ 0 \;\leq\; S(x,t) &\leq S_c(x)\ . \end{cases} \tag{3}$$

$\mathscr{G}$ (Figure 2a) is the function defined in $[0,1]$ by $\mathscr{G}(u) = \mathscr{H}(u-1)$, $\mathscr{R}$ is the ramp function (Figure 2b) defined in $\mathbb{R}$ by $\mathscr{R}(u) = u\ \mathscr{H}(u)$, where $\mathscr{H}$ is the Heaviside step function (Figure 2c):

$$\begin{aligned} \mathscr{H}: \quad \mathbb{R} &\longrightarrow \{0,1\} \\ u &\longmapsto \begin{cases} 0 \quad \text{if} \quad u < 0 \\ \\ 1 \quad \text{if} \quad u \geq 0\ . \end{cases} \end{aligned} \tag{4}$$

In fact, system (3) can be readily expressed as a partition formulation by rewriting its first two equations:

$$\begin{cases} \dfrac{\partial S}{\partial t}(x,t) &= \left(1-\mathscr{G}\left(\frac{S(x,t)}{S_c(x)}\right)\mathscr{H}\left(-\dfrac{\partial Q}{\partial x}(x,t)+N(t)\,w(x)\right)\right)\left(-\dfrac{\partial Q}{\partial x}(x,t)+N(t)\,w(x)\right) \\ q_S(x,t) &= \left(\mathscr{G}\left(\frac{S(x,t)}{S_c(x)}\right)\mathscr{H}\left(-\dfrac{\partial Q}{\partial x}(x,t)+N(t)\,w(x)\right)\right)\left(-\dfrac{\partial Q}{\partial x}(x,t)+N(t)\,w(x)\right). \end{cases} \tag{5}$$

It is the quantity $\mathscr{G}\big(S/S_c\big)\mathscr{H}\big(-\partial Q/\partial x + N\,w\big)$ that triggers the dynamic transitions between the two regimes. When it is null, system (3) reduces to (1). When it is equal to 1, system (3) reduces to (2).

The fourth line of system (3) ensures that the subsurface water storage S remains positive and lower than S_c.

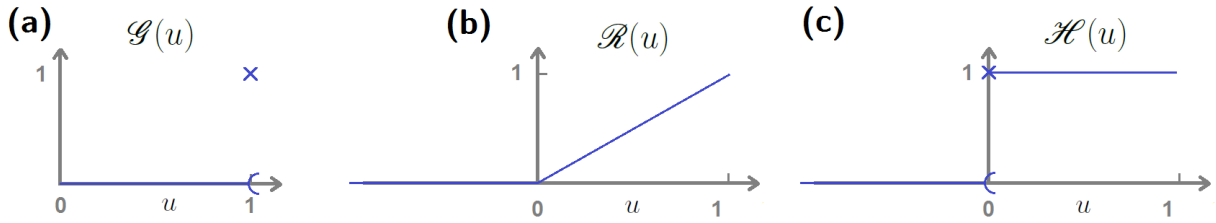

Figure 2: Illustration of (a) the discontinuous function $\mathscr{G}$ (b) the ramp function $\mathscr{R}$ (c) the Heaviside function $\mathscr{H}$ defined by equation (4).

2.3. Numerical methods

System (3) is a set of partial differential equations with discontinuous right-hand sides which can be formally defined in the weak sense of distributions. To solve the partial differential system (3) numerically, $\mathscr{G}$ is challenging because of its discontinuity at $u = 1$. Various numerical techniques exist to handle

the discontinuous functions present in partial derivatives systems (Agosti et al., 2015; Bouillard et al., 2007; Kumar et al., 2014; Hoffmann et al., 2016). System (3) can be rewritten, still in a weak sense, as a non linear complementarity problem, solved with a semi-smooth Newton method (Pang & Gabriel, 1993; De Luca et al., 1996). Here, to solve system (3), we choose to regularize the discontinuous function $\mathscr{G}$, discretize in space using a mixed finite element method and use classic methods for temporal integration (variable-step, variable-order solver).

2.3.1. Regularization

To smoothen the transition between partially and fully saturated regimes, we use the convex function $\mathscr{G}_r$ (Haddou & Migot, 2015) defined by: :

$$\begin{array}{rccl} \mathscr{G}_r : & [0,1] & \longrightarrow & [0,1] \\ & u & \longmapsto & \exp\left(-\dfrac{1-u}{r}\right) \end{array} \tag{6}$$

where $r > 0$. The regularized function $\mathscr{G}_r$ converges to $\mathscr{G}$ when r tends to 0. The function $\mathscr{G}_r$ is continuous in $[0,1]$, convex and differentiable in $[0,1[$. The left derivative in 1 ($\lim_{\substack{x\to 1\\ x<1}} \mathscr{G}_r'(x) = \mathscr{G}_r'(1^-) = \frac{1}{r}$) ensures a sharp transition between the partially and fully saturated regimes. The regularization coefficient $r > 0$ controls the stiffness of the transition between the two states (Figure 3).

Replacing the discontinuous function $\mathscr{G}$ by its continuous counterpart $\mathscr{G}_r$ leads to the system:

$$
\begin{cases}
\dfrac{\partial S}{\partial t}(x,t) + q_S(x,t) &= -\dfrac{\partial Q}{\partial x}(x,t) + N(t)\,w(x) \\
q_S(x,t) &= \mathscr{G}_r\left(\frac{S(x,t)}{S_c(x)}\right)\mathscr{R}\left(-\dfrac{\partial Q}{\partial x}(x,t) + N(t)\,w(x)\right) \\
Q(x,t) &= -\dfrac{kS(x,t)}{f}\left(\cos\theta\ \dfrac{\partial}{\partial x}\left(\dfrac{S}{fw}\right)(x,t) + \sin\theta\right) \\
0 \leq S(x,t) &\leq S_c(x)
\end{cases}
\tag{7}
$$

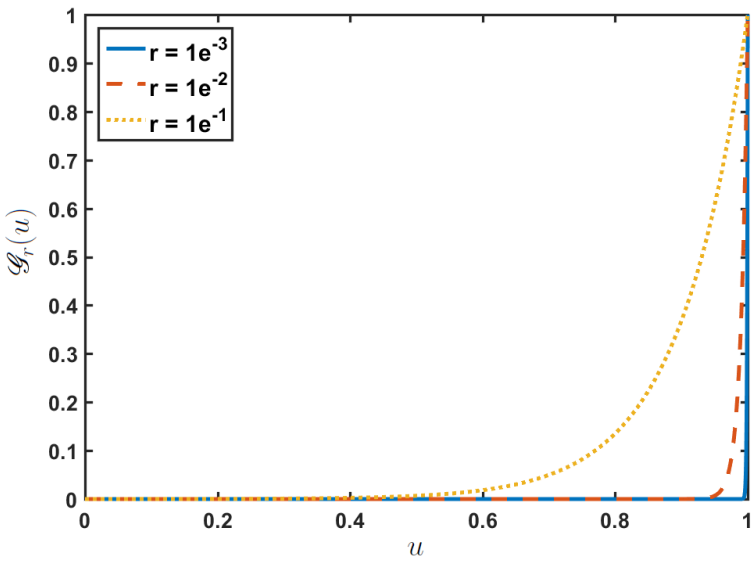

Figure 3: Function $\mathscr{G}_r$ regularized from function $\mathscr{G}$ (figure 2). Function $\mathscr{G}_r$ is defined by equation (6) and represented for different values of the regularization parameter r.

2.3.2. Space and time discretization

We discretize the 1D hillslope in N_x elements and use a mixed finite element method to derive from the system (7) estimates of the soil storage S, the subsurface flux Q and the excess overland flux q_S (Douglas & Roberts, 1985). S and q_S are discretized at the cell centers and Q at their edges following the

classic mixed finite element methodology. As for regular grids, finite differences lead to the same expression as mixed finite element (Chavent & Roberts, 1991), we express spatial derivatives by their finite difference approximation. In practice, the continuity equation (third equation in system 7) is discretized at the cell centers and the integrated Darcy equation (second equation of system 7) is discretized at the edges. Q and $\frac{\partial}{\partial x}\left(\frac{S}{fw}\right)$ are defined at the cell edges by imposing their continuity between two adjacent cells. The multiplicative factor $\frac{kS}{f}$ at the cell edge is taken as the arithmetic average between the neighboring cell centres. The discretization in space of the system (7) eventually leads to a semi-discrete system of ordinary differential equations. We use the variable time step and variable order ode15s MATLAB® solver based on the backward differentiation formulas (BDF) of orders 1 to 5 (Shampine et al., 1999).

2.3.3. Metrics for convergence analysis

We define the metrics for the convergence analysis of the discretization scheme using a discrete L^2 norm. Let $\{t_i,\ i = 1, \cdots, N_t\}$ a set of given times in $[0, T]$ with $t_0 = 0$ and $\{x_k,\ k = 1, \cdots, N_{ref}\}$ a set of given points in $[0, L]$ with $x_0 = 0$. We define the discrete norm of a function $f(x, t)$ with given values $f(x_k, t_i)$ by:

$$\|f\|^2 = \sum_{i=1}^{N_t} \sum_{k=1}^{N_{ref}} |f(x_k, t_i)|^2 \, (t_i - t_{i-1}) \, (x_k - x_{k-1}) \tag{8}$$

In order to compare a function f with a reference function g, we introduce the relative error metric ϵ_f defined by:

$$\epsilon_f = \frac{\|f - g\|}{\|g\|} \tag{9}$$

with adapted computations when f and g display different spatial discretization schemes. In practice, the times t_i are provided by user-defined external time-steps and the points x_k are cell centers or cell edges of a reference mesh.

3. Results

We assess the partition formulation (7) discretized with a mixed finite element scheme on several numerical experiments. We use two numerical experiments of Troch et al. (2003) without any overland flow generated for the first one, and with locally saturated hillslope for the second one. ~~First, we use one of the numerical experiments of Troch et al. (2003) where no overland flow is generated. Then we use a numerical experiment of Troch et al. (2003) where the hillslope saturates locally.~~ We also design experiments with transitions from purely subsurface flow dynamics to simultaneous subsurface and saturation excess overland flows. On this latter experiment, we exhibit that the choice of the discretization scheme preserves the mass balance, we determine the convergence of the spatial discretization scheme, analyze the internal time steps influence and assess the sensitivity of the partition formulation to the regular-

ization parameter r. Third we carry extensive numerical testing to assess the robustness of the regularized partition formulation on realistic experiments.

3.1. Comparison with previous numerical experiments

3.1.1. Case without overland flow

We check the partition formulation (7) on the numerical experiments of Troch et al. (2003). We choose the straight hillslope experiments with a slope of 5% as it is the less likely to fully saturate the soil column and to generate saturation excess overland flow. For this case, boundary conditions are $S(x = 0, t) = 0$ at the channel outlet and $Q(x = L, t) = 0$ at the water divide. The hillslope is 100 m long, spatially discretized with $N_x = 100$ elements. We apply a regularization parameter $r = 1 \times 10^{-3}$ and consider two infiltration cases. The first case is a recharge experiment with a constant infiltration ($N = 10$ mm d^{-1}) on an initially dry hillslope ($S(x, t = 0) = 0$). The second case is a free drainage experiment ($N = 0$ mm d^{-1}) on a hillslope initially partially saturated (uniformly saturated at 20% of its maximum capacity i.e. $S(x, t = 0) = 0.2 \times S_c(x)$).

Figure 4 shows a close agreement of the two methods in both recharge and drainage experiments with the marked storage accumulation near the river (left part of the graphs). The sharp saturation gradient next to the river comes from the imposed Dirichlet condition of zero storage at the river. This test demonstrates the consistency of our numerical approximation of system (7) with the method of Troch et al. (2003) which is based on the discretization of

system (1).

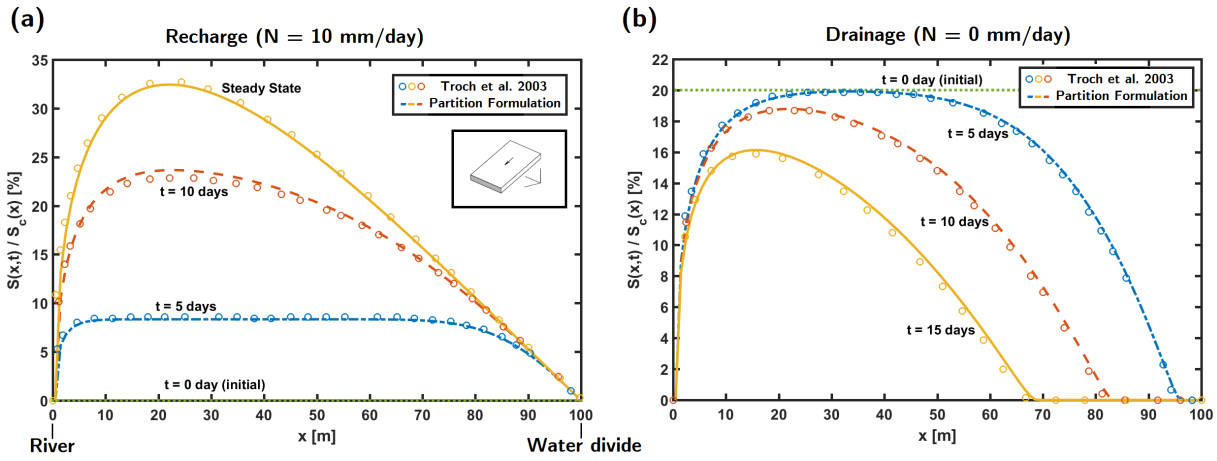

Figure 4: Relative subsurface water storage $S(x,t)/S_c(x)$ (expressed in %) along the hillslope for the (a) recharge and (b) drainage experiments. Insert shows a sketch of the hillslope of slope 5% (Troch et al., 2003).

3.1.2. Case with overland flow

We further assess the partition formulation on a steep convergent hillslope (insert of Figure 5, slope of 30%, Troch et al. (2003)). The hillslope saturates close to its outlet. It is initially partially saturated, $S(x, t = 0) = 0.2\, S_c(x)$, and progressively drains to the river where the saturation remains imposed $S(x = 0, t) = 0$. Hillslope is limited on its upper side by a water divide condition $Q(x = L, t) = 0$.

The saturation profiles and the subsurface flow to the river remain close to those of Troch et al. (2003) (Figure 5). The main benefit of the partition formulation (7) is to provide the saturation excess overland flow generated both spatially and temporally, which amounts to 16% of the total outflow to the river (Figure 5b). The river outflow is not bounded by the limited interface of the

subsurface to the river in this convergent configuration. It may be significantly enhanced by the generation of saturation excess overland flow when the water table intercepts the land surface (Figure 5b).

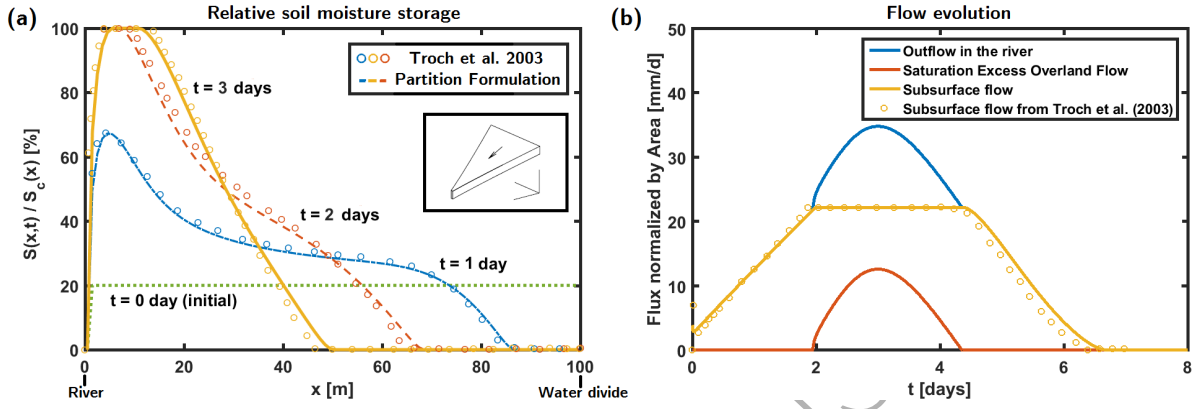

Figure 5: (a) Relative subsurface water storage $S(x,t)/S_c(x)$ (expressed in %) along the 30% sloping convergent hillslope shown in the insert (Troch et al., 2003) during the drainage of partially saturated initial conditions. (b) Outflow evolution in the river for the same drainage experiment.

3.2. Saturation excess overland flow on a convergent hillslope

To check that the saturation excess overland flow is well modeled, we consider a steep periodic hydrologic forcing $N(t)$ on a hillslope with another convergent shape (shown in insert of Figure 6, Troch et al. (2003)). Both the convergence of the hillslope and the high value of infiltration tend to generate saturation excess overland flow with dynamically generated fully saturated areas. Boundary conditions are modified at the river to fully saturated soil ($S(x=0,t)=S_c(x)$) but remain no flow at the water divide ($Q(x=L,t)=0$). Initially, the hillslope is dry ($S(x,t=0)=0$). $N(t)$ is a square wave with a period of 10 days and values alternating between 0 and 30 mm d^{-1}. We spatially discretize the hillslope

with $N_x = 100$ elements and apply a regularization parameter $r = 1 \times 10^{-3}$.

Starting from dry conditions, hillslope progressively fills with quickly rising saturation next to the river because of the convergence conditions (Figure 6a or Video 1). The saturation profile at $t = 12$ days does not show any seepage while at $t = 26$ days and at $t = 35$ days, an extended seepage front has developed in the 20 m next to the river. Even though saturation profiles are close at $t = 26$ days and $t = 35$ days, seepage is almost twice as large at $t = 26$ days because of the presence of direct precipitations onto saturated areas (Figure 6b or Video 1). At $t = 35$ days, only seepage flow occurs. Breakdown of the mass balance at the hillslope scale shows the partition of the incoming infiltration in global storage variations, saturation excess overland flow generated and outflow in the river (Figure 7 or Video 1). Despite the intermittent infiltration, the discharge in the river is steadily increasing because of the progressive filling of the hillslope after the dry initial conditions. Discharge in the river remains always larger than the saturation excess overland flow.

3.2.1. Mass balance error analysis

Interest of the mixed finite element scheme is to preserve mass balance at the scale of the discretized spatial elements. A detailed analysis of the local mass balance error with the numerical experiment described previously shows that statistics (mean and 99^{th} percentile) carried on the spatial and temporal distributions of the mass balance errors are of the order of 10^{-13} m^3 s^{-1} and

Video 1: Video representing (a) the temporal evolution of the terms of the hillslope mass balance (infiltration, storage, river discharge, saturation excess overland flow) and the total mass balance error (b) the subsurface water storage profile measured on the left axis (blue line) and the saturation excess overland flow measured on the right axis (red line). River is on the left at x=0 m, hillslope divide is on the right at x=100 m.

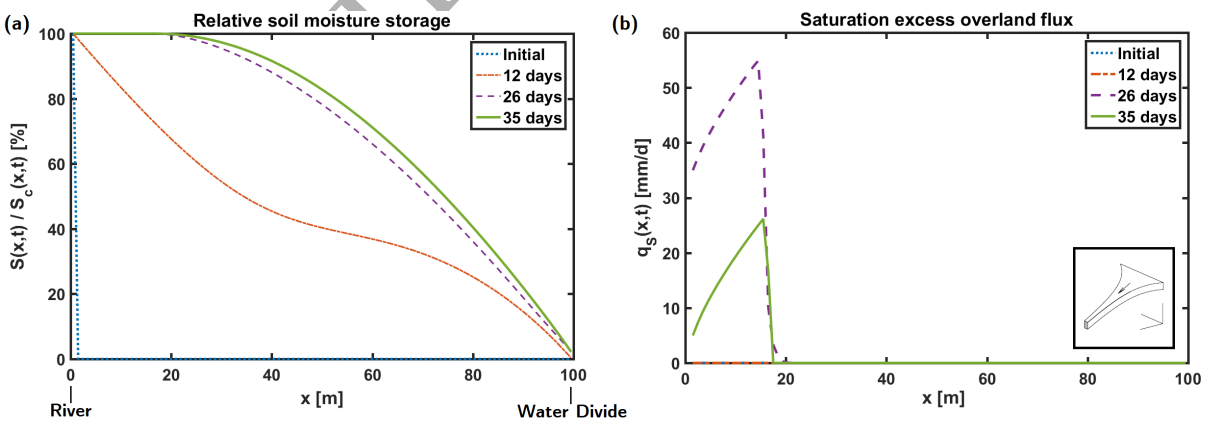

Figure 6: (a) Subsurface water storage and (b) Saturation excess overland flow profile along a convergent hillslope. Sketch of the convergent hillslope is shown in the insert (Troch et al., 2003).

320 remain smaller than the tolerance of the ode15s solver (absolute tolerance fixed
321 at 10^{-10} m^3 s^{-1}). When normalized by the forcing terms (second line of table
322 1), mass balance errors are not found significative (in average equal to $1.6 \times$
323 10^{-7}). Thus the applied spatial discretization scheme guarantees local mass
324 conservation. At the scale of the entire hillslope, Figure 7 illustrates this mass
325 balance preservation globally.

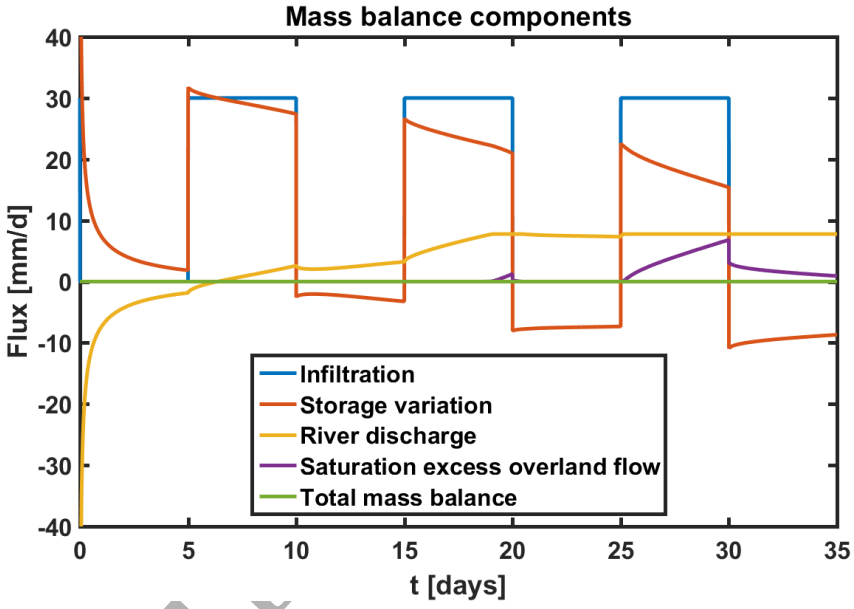

Figure 7: Temporal evolution of the terms of the hillslope mass balance (first equation in system 7) in terms of storage variation, river discharge and saturation excess overland flow. The sum of the terms (the mass balance error) remains equal to 0.

	mean	std	1^{st} %ile	99^{th} %ile
Mass balance [$m^3.s^{-1}$]	3.0×10^{-13}	6.0×10^{-12}	0	3.8×10^{-13}
Normalized Mass balance [-]	1.6×10^{-7}	3.2×10^{-6}	0	2.0×10^{-7}

Table 1: First line: statistics on the mass balance error [m^3 s^{-1}] for the 100 discretized elements of the hilslope. Second line: normalized mass balance statistics [-] adimensioned by the rainfall (30 mm d^{-1}). Absolute tolerance of the ode15s solver was set to 10^{-10} for this numerical experiment.

3.2.2. Convergence with the spatial discretization

Following the convergence metrics defined in equation (9), we compare different simulations of the same numerical experiments with N_x varying between 300 and 700 to the reference simulation composed of 1100 cells. The regularization parameter r is fixed to 1×10^{-3}. Thus we determine the convergence rate $\epsilon_{Q_{N_x}}$ as a function of N_x. We show the convergence results only for Q (figure 8) as they are similar for S and q_S. It shows a fast increase in precision compared to the reference solution. The magnitude of the slope in a log/log scale is equal to -0.95. Convergence rate is close to the theoretical rate equal to -1 demonstrated for linear and smooth problems, $\epsilon_{Q_{N_x}} = O(\frac{1}{N_x})$ (Chavent & Roberts, 1991).

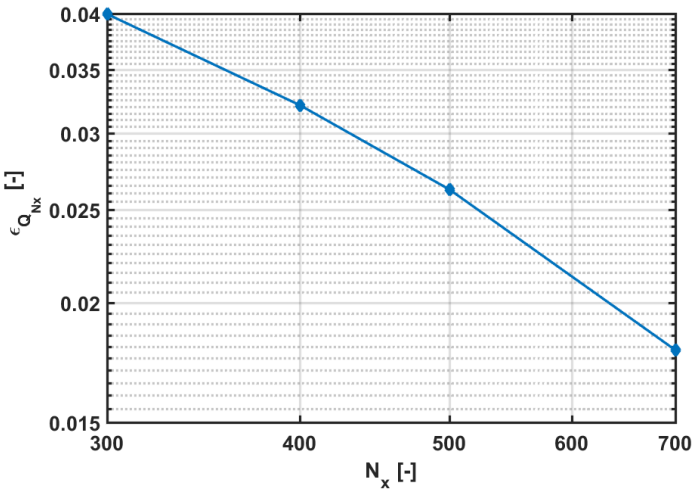

Figure 8: Spatial convergence analysis of Q on the convergent hillslope. Simulations with N_x varying from 100 to 1000 are compared to the reference simulation with $N_x = 1100$. The error metric $\epsilon_{Q_{N_x}}$ is defined by equation (9).

3.2.3. Time steps analysis

Accuracy is also obtained by adapting the time step and the order of the scheme in ode15s to solve system (7). Figure 9a shows that the total number of internal timesteps n_t increases approximately linearly with N_x ($n_t \simeq 40N_x$). The adaptive method used by ode15s is efficient to provide optimal balance between accuracy and efficiency. We cannot separate the effects of the spatial discretization from the number of computed internal timesteps on the gain in accuracy as we use the integrated solver ode15s which automatically adapts its timesteps. Figure 9b highlights at which time ode15s refines its internal timesteps during the simulation. It shows the cumulated number of internal timesteps used by ode15s as a function of the time simulated for different spatial discretization (N_x between 100 and 700). The number of internal timesteps increases rapidly at the beginning of the simulation (for $t < 5$ days) and juste after the infiltration events ($t \geq 10$, 20 or 30 days). These refinements are due to strong gradients appearing in the soil matrix at the beginning of the simulation when the hillslope discretized elements equilibrates with the fixed saturated channel bank and when the infiltration stops. The more the hillslope is discretized, the more pronounced is the refinement. This may be to satisfy the relative error tolerance which is more difficult to attain for finer discretizations.

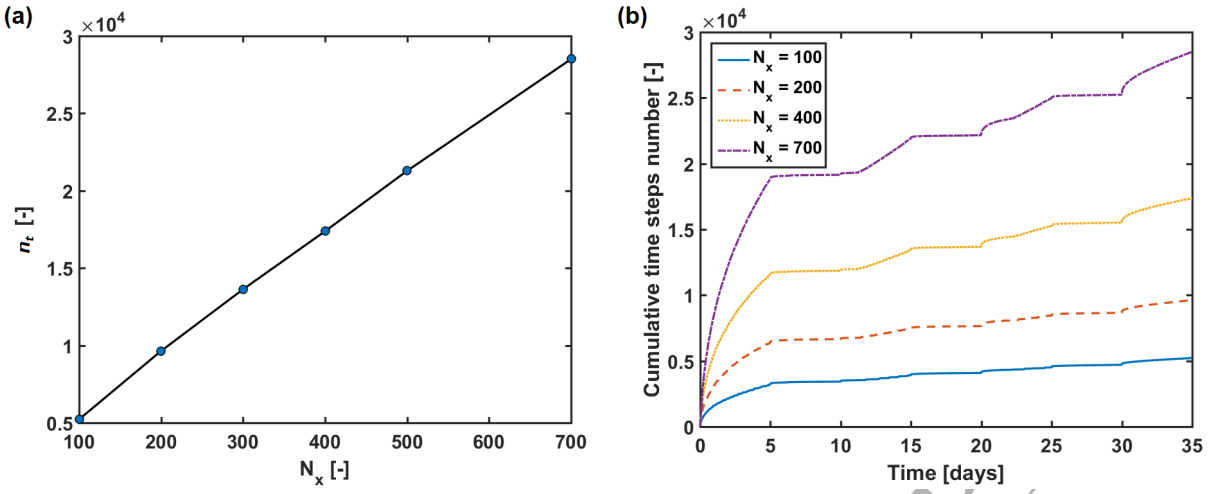

Figure 9: (a) Total number of internal timesteps n_t used by ode15s as a function of the number of the elements N_x used to discretize the hillslope. (b) Evolution of the cumulative number of internal timesteps used by ode15s during a simulation for different numbers of cells N_x.

3.2.4. Convergence with the regularization parameter r

We also determine the convergence rate of ϵ_{S_r} and $\epsilon_{q_{S_r}}$ as a function of the regularization parameter r (equation (9)) for a fixed spatial discretization with $N_x = 100$. The number r varies between 0.2 and 10^{-6} and is compared to the reference solution with $r_{ref} = 2 \times 10^{-7}$ ($N_{ref} = N_x = 100$). We only consider ϵ_{S_r} and $\epsilon_{q_{S_r}}$ since the regularization parameter controls the presence or absence of saturation excess overland flux depending on soil saturation. ϵ_{S_r} and $\epsilon_{q_{S_r}}$ scale with $r^{1.4}$ and $r^{0.94}$ demonstrating the fast convergence with the regularization parameter r. The built-in ode15s solver performs well even with stiff partition functions ($r = 2 \times 10^{-7}$).

We have assessed the numerical methods proposed in section 2.1. The mixed finite element method gives an accurate estimation of fluxes and subsurface

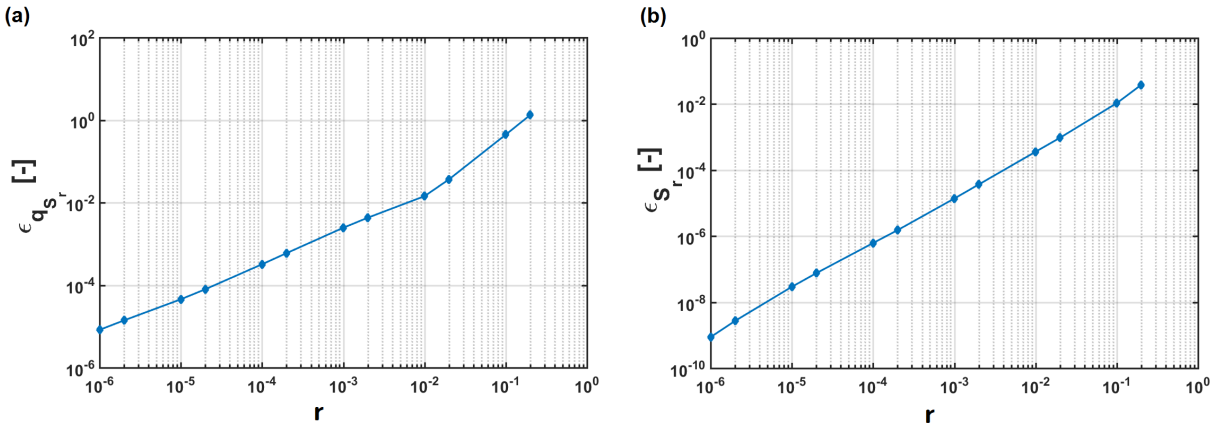

Figure 10: Convergence of (a) q_S and (b) S with the regularization parameter r. Errors are compared to the reference solution taken at $r = 2 \times 10^{-7}$.

water storage, as shown by the comparison with the previous results of Troch et al. (2003). It ensures accurate local and global mass balance preservation. The partition formulation with discontinuous functions and the proposed regularization are relevant methods to account for seepage in efficient and simple ways. They are well suited to follow dynamic transitions between partially and fully saturated regimes. They show good convergence rates with the regularization parameter and lead to problems that can be integrated with classic ordinary differential equation solvers.

3.3. Extensive testing for robustness evaluation

To evaluate the robustness of the method, we run realistic simulations on 1109 real hillslope shapes, with varied geologic parametrizations and with five different infiltration time series. This represents 8320 simulations. Hillslope structures are extracted from a 5m LiDAR Digital Elevation Model of Brittany. Hillslope shapes can be classified in the two categories of the head basin hill-

slopes (Figure 11a) and the riverside hillslopes (i.e. the hillslopes located along river channels, Figure 11b). Head basins hillslopes have a typical divergent and then convergent shape favoring the apparition of saturated source areas near the streams. Hillslopes located along river channels are mainly divergent. Both hillslope types display some complexities in their width functions. Several geologic parametrizations are tested with different values of hydraulic conductivities, soil depths and drainable porosities. These parameters are drawn from truncated lognormal distributions for the hydraulic conductivity and the soil depth and from a truncated normal distribution for drainable porosity (Table 2). Infiltration time series are taken as simple synthetic cases or deduced from real precipitations. The two synthetic cases are a steady infiltration time series of 0.75 mm d^{-1} and a square periodic (period of 10 days) infiltration time series of 35 days varying between 0 and 1.5 mm d^{-1}. Three realistic infiltration cases are derived from three different precipitation chronicles of 15, 61 and 365 days. For the steady infiltration time series, we start the simulation from an initially dry soil profile. For the other infiltration time series, we take the steady subsurface water storage profile under the average infiltration of the time series as initial conditions.

Figure 12 illustrates the simulation methodology for a 1 km^2 hillslope of the Pleine Fougeres watershed (Kolbe et al., 2016) located in North Brittany (Figure 12a) with the realistic 61 days infiltration time series (Figure 12b). Hy-

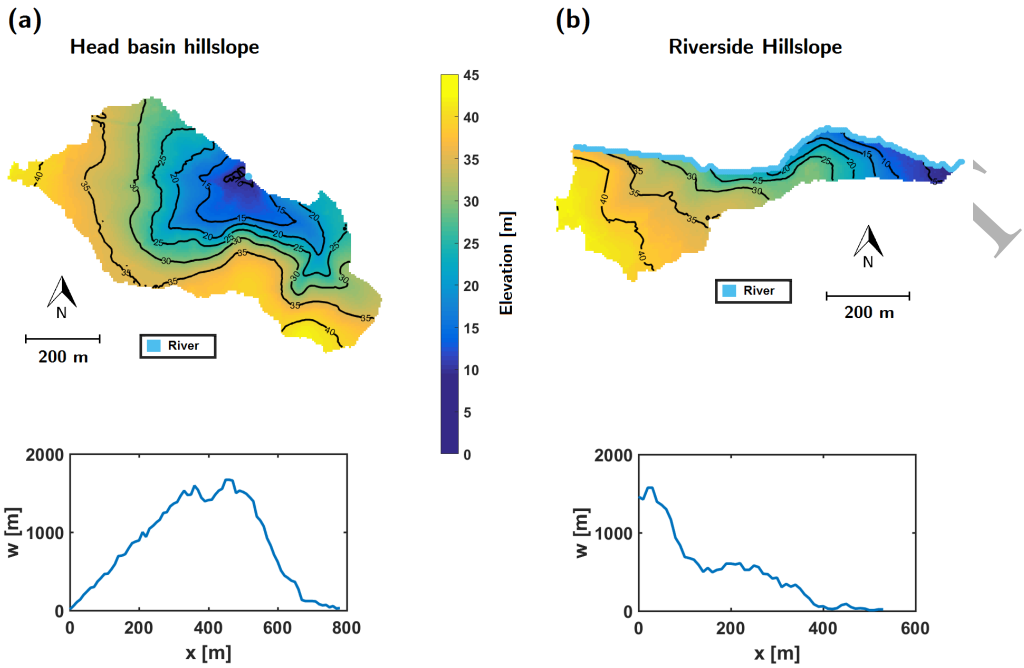

Figure 11: Two major classes of hillslopes: (a) Head basin hillslopes located at the spring of river. (b) Riverside hillslopes located along the river channel. Notice the different behaviour of their width functions.

Parameters	Distribution type	mean	std	Interval
f [%]	Normal	30	10	[5,50]
k [m h^{-1}]	Log Normal	1	10	[0.05,15]
d [m]	Log Normal	1	10	[0.2,11]

Table 2: Parameters of the truncated distributions used for the parametrization of the geological properties f (drainable properties), k (hydraulic conductivity) and d (soil depth). Intervals indicate the truncation range.

draulic conductivities, soil depth and drainable porosity are respectively set at 1 m/h, 2 m and 10%. The simulation exhibits a coexistence of subsurface flow along with saturation excess overland flow with two different dynamics (Figure 12c). Subsurface flow dynamic displays smooth response following infiltration events while saturation excess overland flow, made up of both seepage flow and direct precipitations onto saturated areas, responds instanteneously to infiltrations with highly peaked flows. Out of the 8320 cases tested, no errors were reported by the MATLAB® ode15s solver. These extensive numerical experiments on contrasted hillslopes with sharp infiltration times series demonstrate the robustness of the numerical methods proposed, even in the case of steep rainfall time series (Figure 12).

4. Conclusion

Hillslope response to precipitations is characterized by sharp transitions between two different regimes defined as a function of soil saturation. For partial soil column saturation, flows are restricted to the subsurface. For fully saturated soil column, flows occur both in the subsurface and on the surface as saturation excess overland flow. The hillslope response is highly impacted by the dynamic transition between these regimes. We propose a partition formulation with a mass balance equation where the storage variation is equal to the sum of the local variation of the infiltration and the subsurface flow minus the overland flow. We derive a regularized model which can be discretized in space and time by

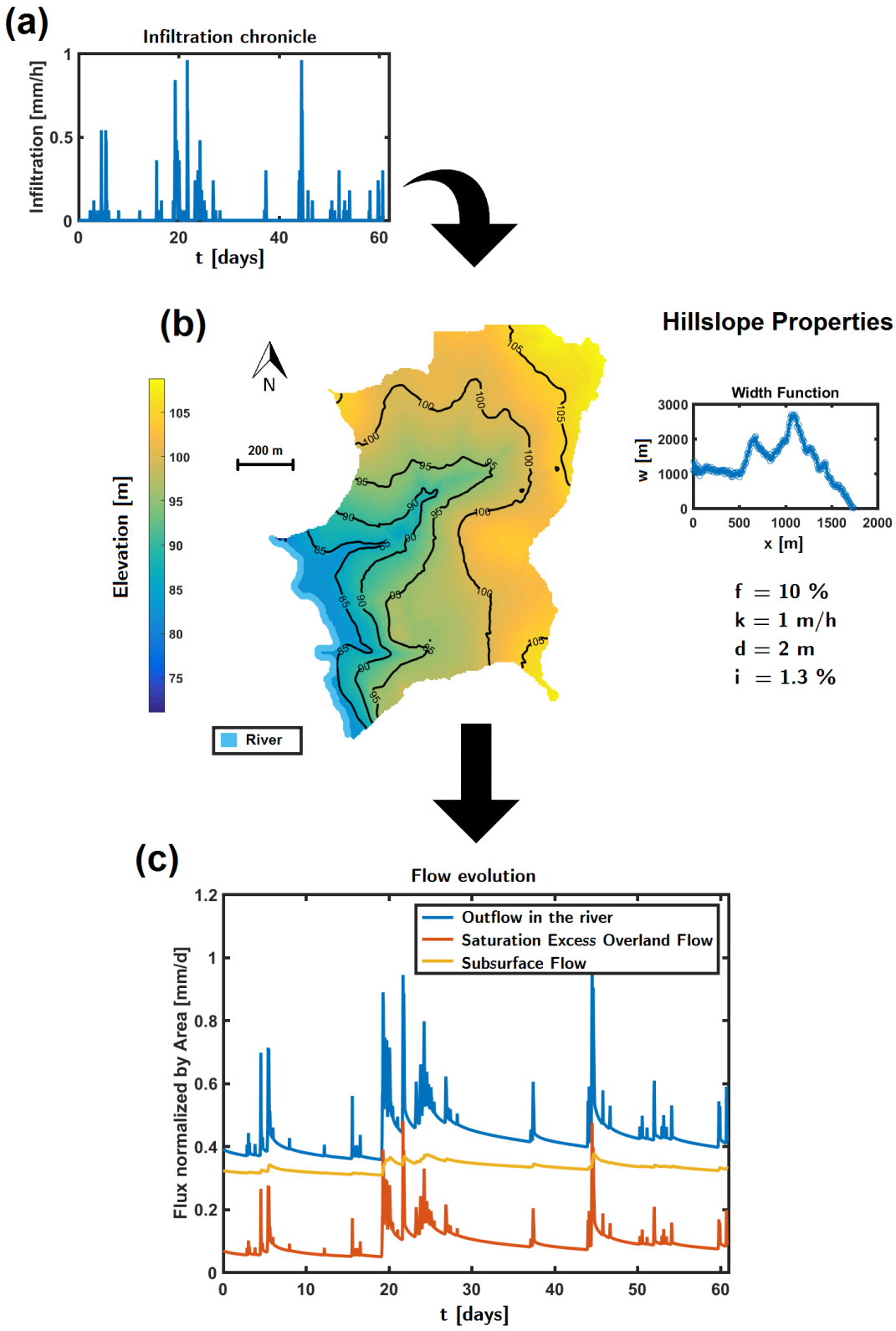

Figure 12: Results of the simulation for a real hillslope from a catchment in Brittany (France) (Kolbe et al., 2016) with (a) the infiltration chronicle, (b) the hillslope shape and properties (width function and pedologic parameters) and (c) the hillslope response as subsurface and saturation excess overland flow and the sum of both (outflow in the river).

classic schemes. We choose a mixed finite element method which ensures local and global mass balance preservation along with an implicit temporal scheme to deal with sharp transitions.

The regularized discrete scheme has been validated against previously published results without saturation excess overland flow. With saturation excess overland flow, additional numerical experiments on a convergent hillslope show good convergence properties for both flow and saturation. Extensive tests on 8320 cases with different hillslope shapes and infiltration time series demonstrate the overall robustness of the method. The regularized and discretized partition formulation thus appears accurate and robust.

This model may be especially relevant for hillslopes with steep, shallow and conductive soils on top of poorly weathered bedrocks that promote the generation of saturation excess overland flow in riparian areas where surface flow routing can be neglected (Weiler et al., 2006). These conditions are typically encountered in Brittany (Merot et al., 2003; Montreuil & Merot, 2006). Integrating this model at the regional scale requires to subdivide the watershed into representative sub-units hillslopes. This can be done by automatically extracting contour-based hillslopes (Moretti & Orlandini, 2008) based on the representative elementary watersheds (Reggiani et al., 1998).

More generally this formulation provides a well-established mathematical formulation for dynamic transitions between partially and fully saturated regimes.

It might be extended to 2D shallow aquifers. Adapted partition conditions might also be formulated for shallow water equations on top of 2D Boussinesq subsurface flows with the additional capacity to account for reinfiltration processes.

Acknowledgements:

We thank Tangi Migot and Mounir Haddou for insightful discussions. Work was partly funded by the project H2MNO4 under the №ANR-12-MONU-0012-01.

References

Agosti, A., Formaggia, L., & Scotti, A. (2015). Analysis of a model for precipitation and dissolution coupled with a darcy flux. *Journal of Mathematical Analysis and Applications*, *431*, 752–781. doi:10.1016/j.jmaa.2015.06.003.

Anderson, M. P., Woessner, W. W., & Hunt, R. J. (2015). *Applied groundwater modeling: simulation of flow and advective transport*. Academic press, Second edition.

Bachmair, S., & Weiler, M. (2012). Hillslope characteristics as controls of subsurface flow variability. *Hydrol. Earth Syst. Sci.*, *16*, 3699–3715. doi:10.5194/hess-16-3699-2012.

Barthel, R., & Banzhaf, S. (2016). Groundwater and surface water interaction at the regional-scale - a review with focus on regional integrated models. *Water Resource Management*, *30*, 1–32. doi:10.1007/s11269-015-1163-z.

Batelaan, O., & De Smedt, F. (2004). Seepage, a new modflow drain package. *Ground Water*, *42*, 576–588. doi:10.1111/j.1745-6584.2004.tb02626.x.

Bauer, P., Gumbricht, T., & Kinzelbach, W. (2006). A regional coupled surface water/groundwater model of the Okavango Delta, Botswana. *Water Resources Research*, *42*. doi:10.1029/2005WR004234.

Beaugendre, H., Ern, A., Esclaffer, T., Gaume, E., Ginzburg, I., & Kao, C. (2006). A seepage face model for the interaction of shallow water tables with the ground surface: Application of the obstacle-type method. *Journal of Hydrology*, *329*, 258–273. doi:10.1016/j.jhydrol.2006.02.019.

Beven, K. (2006). A manifesto for the equifinality thesis. *Journal of Hydrology*, *320*, 18 – 36. doi:http://dx.doi.org/10.1016/j.jhydrol.2005.07.007.

Birkel, C., Soulsby, C., & Tetzlaff, D. (2015). Conceptual modelling to assess how the interplay of hydrological connectivity, catchment storage and tracer dynamics controls nonstationary water age estimates. *Hydrological Processes*, *29*, 2956–2969. doi:10.1002/hyp.10414.

Bishop, K., Seibert, J., Nyberg, L., & Rodhe, A. (2011). Water storage in a till catchment. II: Implications of transmissivity feedback for flow paths and turnover times. *Hydrological Processes*, *25*, 3950–3959. doi:10.1002/hyp.8355.

Bonell, M. (1998). Selected challenges in runoff generation research in forests from the hillslope to headwater drainage basin scale. *Journal of the American Water Resources Association*, *34*, 765–785. doi:10.1111/j.1752-1688.1998.tb01514.x.

Bouillard, N., Eymard, R., Herbin, R., & Montarnal, P. (2007). Diffusion with dissolution and precipitation in a porous medium: Mathematical analysis and numerical approximation of a simplified model. *ESAIM - Mathematical Modelling and Numerical Analysis - Modélisation Mathématique et Analyse Numérique*, *41*. doi:10.1051/m2an:2007047.

Boussinesq, J. (1877). *Essai sur la théorie des eaux courantes*. Mémoires présentées par divers savants à l'Académie des Sciences, Extrait des tomes XXIII et XXIV. Imprimerie Nationale.

Bresciani, E., Davy, P., & de Dreuzy, J.-R. (2014). Is the Dupuit assumption suitable for predicting the groundwater seepage area in hillslopes? *Water Resources Research*, *50*, 2394–2406. doi:10.1002/2013WR014284.

Bresciani, E., Goderniaux, P., & Batelaan, O. (2016). Hydrogeological controls of water table-land surface interactions. *Geophysical Research Letters*, *43*, 9653–9661. doi:10.1002/2016GL070618.

Broda, S., Larocque, M., Paniconi, C., & Haitjema, H. (2012). A low-dimensional hillslope-based catchment model for layered groundwater flow. *Hydrological Processes*, *26*, 2814–2826. doi:10.1002/hyp.8319.

Brutsaert, W. (2005). *Hydrology: an introduction*. Cambridge University Press.

Camporese, M., Paniconi, C., Putti, M., & Orlandini, S. (2010). Surface-subsurface flow modeling with path-based runoff routing, boundary condition-based coupling, and assimilation of multisource observation data. *Water Resources Research*, *46*, n/a–n/a. doi:10.1029/2008WR007536. W02512.

Chavent, G., & Roberts, J. (1991). A unified physical presentation of mixed, mixed-hybrid finite elements and standard finite-difference approximations for the determination of velocities in waterflow problems. *Advances in Water Resources*, *14*, 329–348. doi:10.1016/0309-1708(91)90020-O.

Darboux, F., Davy, P., Gascuel-Odoux, C., & Huang, C. (2002). Evolution of soil surface roughness and flowpath connectivity in overland flow experiments. *CATENA*, *46*, 125–139. doi:10.1016/S0341-8162(01)00162-X.

De Luca, T., Facchinei, F., & Kanzow, C. (1996). A semismooth equation approach to the solution of nonlinear complementarity problems. *Mathematical Programming*, *75*, 407–439. doi:10.1007/BF02592192.

Diersch, H.-J. (2013). *FEFLOW: finite element modeling of flow, mass and heat transport in porous and fractured media*. Springer Science & Business Media. doi:10.1007/978-3-642-38739-5.

Doherty, J., & Christensen, S. (2011). Use of paired simple and complex models to reduce predictive bias and quantify uncertainty. *Water Resources Research*, *47*. doi:10.1029/2011WR010763. W12534.

Douglas, J., & Roberts, J. (1985). Global estimates for mixed methods for 2nd order elliptic-equations. *Mathematics of computation*, *44*, 39–52. doi:10.1090/S0025-5718-1985-0771029-9.

Dunne, T. (1978). Field studies of hillslope flow processes. *Hillslope hydrology*, *227*, 227–293.

Dunne, T., & Black, R. D. (1970). Partial area contributions to storm runoff in a small new england watershed. *Water Resources Research*, *6*, 1296–1311. doi:10.1029/WR006i005p01296.

Fan, Y., & Bras, R. L. (1998). Analytical solutions to hillslope subsurface storm flow and saturation overland flow. *Water Resources Research*, *34*, 921–927. doi:10.1029/97WR03516.

Fatichi, S., Vivoni, E. R., Ogden, F. L., Ivanov, V. Y., Mirus, B., Gochis, D., Downer, C. W., Camporese, M., Davison, J. H., Ebel, B., Jones, N., Kim, J., Mascaro, G., Niswonger, R., Restrepo, P., Rigon, R., Shen, C., Sulis, M., & Tarboton, D. (2016). An overview of current applications, challenges, and future trends in distributed process-based models in hydrology. *Journal of Hydrology*, *537*, 45 – 60. doi:10.1016/j.jhydrol.2016.03.026.

Fox, G. A., & Wilson, G. V. (2010). The role of subsurface flow in hillslope and stream bank erosion: A review. *Soil Science Society of America Journal*, *74*, 717–733. doi:10.2136/sssaj2009.0319.

Freer, J., McDonnell, J., Beven, K., Brammer, D., Burns, D., Hooper, R., & Kendal, C. (1997). Hydrological processes letters: Topographic controls on subsurface storm flow at the hillslope scale for two hydrologically distinct small catchments. *Hydrological Processes*, *11*, 1347–1352. doi:10.1002/(SICI)1099-1085(199707)11:9<1347::AID-HYP592>3.0.CO;2-R.

Freer, J., McDonnell, J. J., Beven, K. J., Peters, N. E., Burns, D. A., Hooper, R. P., Aulenbach, B., & Kendall, C. (2002). The role of bedrock topography on subsurface storm flow. *Water Resources Research*, *38*, 5–1–5–16. doi:10.1029/2001WR000872. 1269.

Freeze, R. A., & Harlan, R. (1969). Blueprint for a physically-based, digitally-simulated hydrologic response model. *Journal of Hydrology*, *9*, 237–258. doi:10.1016/0022-1694(69)90020-1.

Govindaraju, R. S., & Kavvas, M. L. (1991). Dynamics of moving boundary overland flows over infiltrating surfaces at hillslopes. *Water Resources Research*, *27*, 1885–1898. doi:10.1029/91WR00689.

Habets, F., Gascoin, S., Korkmaz, S., Thiery, D., Zribi, M., Amraoui, N., Carli, M., Ducharne, A., Leblois, E., Ledoux, E., Martin, E., Noilhan, J., Ottle, C., & Viennot, P. (2010). Multi-model comparison of a major flood in the groundwater-fed basin of the Somme River (France). *Hydrology and Earth System Sciences*, *14*, 99–117. doi:10.5194/hess-14-99-2010.

Haddou, M., & Migot, T. (2015). A Smoothing Method for Sparse Optimization over Polyhedral Sets. In H. A. L. Thi, T. P. Dinh, & N. T. Nguyen (Eds.), *Modelling, computation and optimization in information systems and management sciences* (pp. 369–379). Springer volume 359 of *Advances in intelligent systems and computing*. doi:10.1007/978-3-319-18161-5_31 proceedings of the 3rd International conference on modelling, computation and optimization in information systems and management sciences - MCO 2015 - Part 1.

Harbaugh, A. W. (2005). *MODFLOW-2005, the US Geological Survey modular ground-water model: the ground-water flow process*. US Department of the Interior, US Geological Survey Reston, VA, USA.

Harman, C. J. (2015). Time-variable transit time distributions and transport: Theory and application to storage-dependent transport of chloride in a watershed. *Water Resources Research*, *51*, 1–30. doi:10.1002/2014WR015707.

Hilberts, A. G. J., van Loon, E. E., Troch, P. A., & Paniconi, C. (2004). The hillslope-storage boussinesq model for non-constant bedrock slope. *Journal of Hydrology*, *291*, 160–173. doi:10.1016/j.jhydrol.2003.12.043.

Hoffmann, J., Kräutle, S., & Knabner, P. (2016). Existence and uniqueness of a global solution for reactive transport with mineral precipitation-dissolution and aquatic reactions in porous media, .

Holman, I. P., Tascone, D., & Hess, T. M. (2009). A comparison of stochastic and deterministic downscaling methods for modelling potential groundwater recharge under climate change in East Anglia, UK: implications for groundwater resource management. *Hydrogeology Journal*, *17*, 1629–1641. doi:10.1007/s10040-009-0457-8.

Horton, R. E. (1933). The role of infiltration in the hydrologic cycle. *Eos, Transactions American Geophysical Union*, *14*. doi:10.1029/TR014i001p00446.

Kirkby, M. J. (1978). *Hillslope Hydrology*. John Wiley.

Kolbe, T., Marçais, J., Thomas, Z., Abbott, B. W., de Dreuzy, J.-R., Rousseau-Gueutin, P., Aquilina, L., Labasque, T., & Pinay, G. (2016). Coupling 3d groundwater modeling with CFC-based age dating to classify local groundwater circulation in an unconfined crystalline aquifer. *Journal of Hydrology*, *543*, 31–46. doi:10.1016/j.jhydrol.2016.05.020.

Kollet, S. J., & Maxwell, R. M. (2006). Integrated surface–groundwater flow modeling: A free-surface overland flow boundary condition in a parallel groundwater flow model. *Advances in Water Resources*, *29*, 945–958. doi:10.1016/j.advwatres.2005.08.006.

Kreibich, H., & Thieken, A. H. (2008). Assessment of damage caused by high groundwater inundation. *Water Resources Research*, *44*. doi:10.1029/2007WR006621.

Kumar, K., Pop, I. S., & Radu, F. A. (2014). Convergence analysis for a conformal discretization of a model for precipitation and dissolution in porous media. *Numerische Mathematik*, *127*, 715–749. doi:10.1007/s00211-013-0601-1.

LaBolle, E., Ahmed, A., & Fogg, G. (2003). Review of the integrated groundwater and surface-water model (igsm). *Ground Water*, *41*, 238–246. doi:10.1111/j.1745-6584.2003.tb02587.x.

Lanni, C., McDonnell, J., Hopp, L., & Rigon, R. (2013). Simulated effect of soil depth and bedrock topography on near-surface hydrologic response and slope stability. *Earth Surface Processes and Landforms*, *38*, 146–159. doi:10.1002/esp.3267.

Markstrom, S. L., Niswonger, R. G., Regan, R. S., Prudic, D. E., & Barlow, P. M. (2008). GSFLOW-Coupled Ground-water and Surface-water FLOW model based on the integration of the Precipitation-Runoff Modeling System (PRMS) and the Modular Ground-Water Flow Model (MODFLOW-2005). *US Geological Survey techniques and methods*, *6*, 240.

Maxwell, R., & Condon, L. (2016). Connections between groundwater flow and transpiration partitioning. *Science*, *353*, 377–380. doi:10.1126/science.aaf7891.

McGlynn, B. L., McDonnel, J. J., & Brammer, D. D. (2002). A review of the evolving perceptual model of hillslope flowpaths at the maimai catchments, new zealand. *Journal of Hydrology*, *257*, 1–26. doi:10.1016/S0022-1694(01)00559-5.

Tromp-van Meerveld, H. J., & McDonnell, J. J. (2006). Threshold relations in subsurface stormflow: 2. the fill and spill hypothesis. *Water Resources Research*, *42*, W02411. doi:10.1029/2004WR003800.

Merot, P., Squividant, H., Aurousseau, P., Hefting, M., Burt, T., Maitre, V., Kruk, M., Butturini, A., Thenail, C., & Viaud, V. (2003). Testing a climato-topographic index for predicting wetlands distribution along an european climate gradient. *Ecological Modelling*, *163*, 51 – 71. doi:10.1016/S0304-3800(02)00387-3.

Miguez-Macho, G., & Fan, Y. (2012). The role of groundwater in the Amazon water cycle: 1. Influence on seasonal streamflow, flooding and wetlands. *Journal of Geophysical Research - Atmospheres*, *117*. doi:10.1029/2012JD017539.

Montreuil, O., & Merot, P. (2006). Nitrogen removal in valley bottom wetlands. *Journal of Environmental Quality*, *35*, 2113 – 2122. doi:10.2134/jeq2006.0091.

Moretti, G., & Orlandini, S. (2008). Automatic delineation of drainage basins from contour elevation data using skeleton construction techniques. *Water Resources Research*, *44*. doi:10.1029/2007WR006309. W05403.

Musy, A., & Higy, C. (2004). *Hydrologie: Une science de la nature* volume 21. PPUR presses polytechniques.

Ogden, F. L., & Watts, B. A. (2000). Saturated area formation on nonconvergent hillslope topography with shallow soils: A numerical investigation. *Water Resources Research*, *36*, 1795–1804. doi:10.1029/2000WR900091.

Panday, S., & Huyakorn, P. S. (2004). A fully coupled physically-based spatially-distributed model for evaluating surface/subsurface flow. *Advances in Water Resources*, *27*, 361–382. doi:10.1016/j.advwatres.2004.02.016.

Pang, J.-S., & Gabriel, S. A. (1993). Ne/sqp: A robust algorithm for the nonlinear complementarity problem. *Mathematical Programming*, *60*, 295–337. doi:10.1007/BF01580617.

Paniconi, C., Troch, P. A., van Loon, E. E., & Hilberts, A. G. J. (2003). Hillslope-storage boussinesq model for subsurface flow and variable source areas along complex hillslopes: 2. intercomparison with a three-dimensional richards equation model. *Water Resources Research*, *39*, n/a–n/a. doi:10.1029/2002WR001730. 1317.

Pinay, G., Peiffer, S., Dreuzy, J.-R., Krause, S., Hannah, D. M., Fleckenstein, J. H., Sebilo, M., Bishop, K., & Hubert-Moy, L. (2015). Upscaling nitrogen removal capacity from local hotspots to low stream orders' drainage basins. *Ecosystems*, *18*, 1101–1120. doi:10.1007/s10021-015-9878-5.

Putti, M., & Paniconi, C. (2004). Time step and stability control for a coupled model of surface and subsurface flow. *Developments in Water Science*, *55*, 1391–1402. doi:10.1016/S0167-5648(04)80152-7.

Reggiani, P., Sivapalan, M., & Hassanizadeh, S. M. (1998). A unifying framework for watershed thermodynamics: balance equations for mass, momentum, energy and entropy, and the second law of thermodynamics. *Advances in Water Resources*, *22*, 367 – 398. doi:10.1016/S0309-1708(98)00012-8.

Rinaldo, A., Benettin, P., Harman, C. J., Hrachowitz, M., McGuire, K. J., van der Velde, Y., Bertuzzo, E., & Botter, G. (2015). Storage selection functions: A coherent framework for quantifying how catchments store

and release water and solutes. *Water Resources Research*, *51*, 4840–4847. doi:10.1002/2015WR017273.

Rodhe, A. (1987). *The origin of streamwater traced by oxygen-18*. Uppsala University, Department of Physical Geography, Division of Hydrology.

Savenije, H. H. G. (2010). HESS Opinions "Topography driven conceptual modelling (FLEX-Topo)". *Hydrology and Earth System Sciences*, *14*, 2681–2692. doi:10.5194/hess-14-2681-2010.

Shampine, L., Reichelt, M., & Kierzenka, J. (1999). Solving index-1 DAEs in MATLAB and simulink. *SIAM Review*, *41*, 538–552. doi:10.1137/S003614459933425X.

Smith, R. E., & Goodrich, D. C. (2006). Rainfall excess overland flow. In *Encyclopedia of Hydrological Sciences*. John Wiley & Sons, Ltd.

Sophocleous, M. (2002). Interactions between groundwater and surface water: the state of the science. *Hydrogeology Journal*, *10*, 52–67. doi:10.1007/s10040-001-0170-8.

Tetzlaff, D., Birkel, C., Dick, J., Geris, J., & Soulsby, C. (2014). Storage dynamics in hydropedological units control hillslope connectivity, runoff generation, and the evolution of catchment transit time distributions. *Water Resources Research*, *50*, 969–985. doi:10.1002/2013WR014147.

Troch, P., Van Loon, E., & Hilberts, A. (2002). Analytical solutions to a hillslope-storage kinematic wave equation for subsurface flow. *Advances in Water Resources*, *25*, 637–649. doi:10.1016/S0309-1708(02)00017-9.

Troch, P. A., Berne, A., Bogaart, P., Harman, C., Hilberts, A. G. J., Lyon, S. W., Paniconi, C., Pauwels, V. R. N., Rupp, D. E., Selker, J. S., Teuling, A. J., Uijlenhoet, R., & Verhoest, N. E. C. (2013). The importance of hydraulic groundwater theory in catchment hydrology: The legacy of Wilfried Brutsaert and Jean-Yves Parlange. *Water Resources Research*, *49*, 5099–5116. doi:10.1002/wrcr.20407.

Troch, P. A., Paniconi, C., & Emiel van Loon, E. (2003). Hillslope-storage boussinesq model for subsurface flow and variable source areas along complex hillslopes: 1. formulation and characteristic response. *Water Resources Research*, *39*, n/a–n/a. doi:10.1029/2002WR001728. 1316.

Vivoni, E. R., Entekhabi, D., Bras, R. L., & Ivanov, V. Y. (2007). Controls on runoff generation and scale-dependence in a distributed hydrologic model. *Hydrology and Earth System Sciences*, *11*, 1683–1701. doi:10.5194/hess-11-1683-2007.

Weiler, M., McDonnell, J. J., Tromp-van Meerveld, I., & Uchida, T. (2006). Subsurface stormflow. In *Encyclopedia of Hydrological Sciences*. John Wiley & Sons, Ltd.